Investigation of δ-electron emission in collisions of highly charged fast Ne projectiles with carbon-foil targets

G. Schiwietz, J. P. Biersack, D. Schneider, N. Stolterfoht, D. Fink, V. J. Montemayor, and B. Skogvall*

Hahn-Meitner-Institut Gesellschaft mit beschränkter Haftung, Berlin, Glienickerstrasse 100, 1000 Berlin 39, Federal Republic of Germany

(Received 28 August 1989)

The angle and energy dependence of electron emission following the interaction of 70–170-MeV Ne^{q+} ($q=7,10$) projectiles with 20 and 100 $\mu g/cm^2$ carbon foils has been investigated experimentally. Absolute emission yields were determined for ejection angles ranging from 0° to 180° and electron energies from 10 eV to 6 keV for normal-incidence ion beams. The experimental δ-electron spectra are compared to results from a newly developed theoretical model based on a separation of energy loss and angular scattering for secondary electrons.

I. INTRODUCTION

The study of electron emission in ion-foil interactions has become the subject of increasing activity.[1–11] Especially the detection of Auger electrons emitted from a solid target provides information about the elemental composition in the surface region of the material.[12]

An electron spectrum consists primarily of a continuous background of electrons, referred to as δ or secondary electrons, extending up to electron energies of a few keV.[9] Superimposed on this background are peak structures due to the Auger decay of inner-shell excited target atoms. On the low-energy side these structures have a tail corresponding to Auger electrons which have suffered inelastic energy loss in the material.[10,13] The peak positions are determined not only by the initial vacancy configuration, but also by the surface potential[10] and by the chemical properties of the material.[14] For a quantitative determination of the Auger spectrum, a background due to directly ionized inner-shell electrons and valence electrons (or energy transfer to conduction-band electrons) has to be subtracted from the measured electron spectra. The most widely used method to determine the background under an Auger peak is a fit using exponential functions or polynomials. As found by Toburen *et al.*[10] this might lead to wrong results. The spectrum of these background electrons (hereafter referred to as δ electrons) agrees well with theoretical ion-atom collision cross sections if high electron energies (>1 keV) and thin targets (2 $\mu g/cm^2$ carbon) are considered.[9] At lower electron energies the energy loss[3] and multiple scattering[13] of δ electrons comes into play, and at very low energies (<30 eV) plasmon excitation[15] and excitons[16] are expected to influence the intensity of the emitted electrons.

Since the shape of the degraded portion of the Auger spectrum depends on the depth distribution of electron emitters inside the material,[13] it should be possible to determine the depth distribution, if the shape of the background intensity is known. In this paper we investigate δ-electron emission from carbon foils in order to test a simple model for electron emission from solid targets which might give new insights into the understanding of electronic energy transport in dense matter. The model neglects any energy loss and angular deflections of the primary ion as well as δ-electron production due to recoil ions. This is expected to be a good approximation if highly energetic ($\gg 1$ MeV/u) heavy ions are used, as in the present investigation. Such ions lose their energy mainly by ionization, and thus produce electron spectra of high intensity. In Sec. II we explain our experimental method for the determination of absolute doubly differential electron emission yields. The theoretical methods used for the calculation of δ-electron yields are described in Sec. III. The experimental and theoretical results are presented and discussed in Sec. IV.

II. EXPERIMENTAL METHOD AND DATA ANALYSIS

Electrons emitted in the interactions of high-energy Ne ions with C foils were measured as a function of electron energy and ejection angle. All data were taken at the VICKSI heavy-ion accelerator at the Hahn-Meitner-Institut. A magnetically charge-state-analyzed Ne^{q+} beam ($q=7,10$) was collimated to a diameter of less than 2 mm. The beam at normal incidence was then passed through a carbon target (20, 100 $\mu g/cm^2$) in the center of a magnetically shielded scattering chamber, and was finally collected in a Faraday cup. The base pressure in the scattering chamber was about 3×10^{-7} torr. Emitted electrons, energy analyzed with an electrostatic 45° spectrometer,[17,18] were counted during the collection of a preset amount of beam charge. The relative electron-energy resolution was in the range of 4–8 % (full width at half maximum) in the different measurements. After any energy spectrum (10 eV–6 keV) was taken, the analyzer was rotated around the collision center to obtain the angular distribution for electron emission angles from 0° to 180°.

Figure 1 displays electron spectra for ejection angles

 ©1990 The American Physical Society

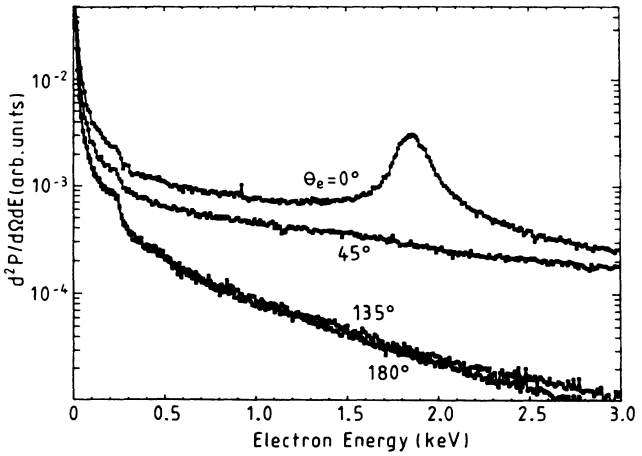

FIG. 1. Measured electron-energy spectra for different ejection angles in 70-MeV Ne^{10+} collisions with a 20 $\mu g/cm^2$ C foil (normal incidence).

from 0° to 180° in collisions of 70-MeV Ne^{10+} projectiles with a 20-$\mu g/cm^2$ C foil. The spectra show a broad continuum and superimposed peak structures at an electron energy of about 250 eV. These structures are due to carbon *KLL* target Auger electrons. In the 0° spectrum at an electron energy of 1.9 keV (equal velocity as the projectile) a major peak is observed. This peak is mainly due to electron capture and electron loss to the projectile continuum, and partially (about 5%) due to highly excited Rydberg electrons field ionized in the electron spectrometer.[18,19]

Figure 2 displays the ratio of the currents measured at the foil and the Faraday cup multiplied by the mean charge state (q_f) of the projectile ions after emerging from the foil. These current measurements were performed as a function of a bias voltage applied to the foil for incident 100-MeV Ne^{10+} and 170-MeV Ne^{7+} projectiles. As the sputtering yield is very small [about 0.1% (Ref. 20)] for such highly energetic projectiles ($v_p \gg v_F$), there is no contribution from sputtered ions. Thus the values in Fig. 2 represent the total number of emitted electrons per incident projectile. The mean charge state q_f was calculated using the empirical formula by Nikolaev and Dmitriev[21] (for further references see the review of Betz[22]):

$$q_f = Z_p(1+2.3Z_p^{0.75}v_p^{-1.67})^{-0.6}\ , \tag{1}$$

where Z_p is the nuclear projectile charge, and v_p the projectile velocity in atomic units. The ratio of the incident charge state to the calculated mean charge state was found to be in good agreement with the ratio of the beam currents measured before (with a well-defined charge state) and after the target foil. The number of emitted electrons (displayed in Fig. 2) decreases from a flat plateau at negative bias potentials to very low values for bias potentials above +50 V. It should be noted that the dependence on the bias potential is not the same as would be obtained from singly differential electron spectra (cf. Fig. 1) since an attractive foil potential may lead to the reabsorption of emitted electrons. An attractive foil contact potential of about 1 eV might also be responsible for the small differences (5–10%) between the number of emitted electrons for zero volts and that for negative bias potentials.

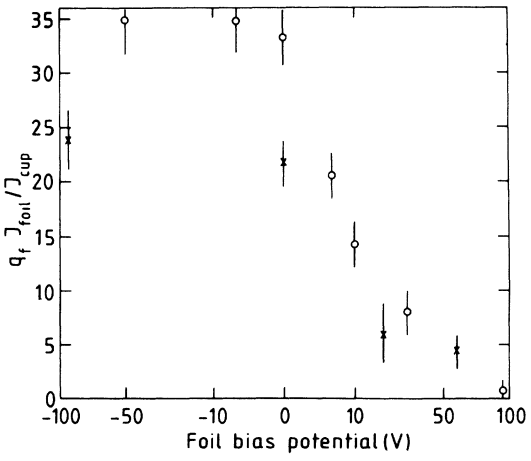

FIG. 2. Number of ejected electrons per incident ion as a function of the foil bias potential. Circles: 100-MeV Ne^{10+} + 20 $\mu g/cm^2$ C foil; crosses: 170-MeV Ne^{7+} + 100 $\mu g/cm^2$ C foil.

In order to obtain absolute doubly differential electron emission yields $d^2P/d\Omega dE$ (number of electrons per incident ion, solid angle, and energy interval) the spectra were corrected for dispersion and integrated (with an uncertainty of about ±20%) over energy (after extrapolation up to the binary encounter energy) and angle of ejection. From a comparison of this value with the number of emitted electrons at zero bias potential we obtained an effective analyzer efficiency (the product of electron energy resolution, solid angle, transparency, and multiplier efficiency). This analyzer efficiency was used to calculate absolute emission yields from the measured spectra. These spectra have an absolute uncertainty of about ±25% and will be presented and discussed in Sec. IV. The relative uncertainty for different data points taken for one collision system is about ±10%.

III. THEORY

In general, the description of the motion of charged particles penetrating a solid is a quantum-mechanical problem of high complexity if all degrees of freedom are taken into account. Perfect crystals are not considered in this paper and thus coherence effects such as, e.g., resonant projectile excitation or ionization,[23] will be of minor importance. We therefore apply a classical transport theory to the problem of electron emission in charged-particle–solid interactions. We assume in this work that the projectile is fast enough so that molecular processes[24] become negligible, and that the projectile energy loss is small compared to the incident energy. In the following we first give a review of the model used to describe the transport of energetic electrons (with high velocities compared to the Fermi velocity) from inside the material to the solid surface. We then describe the atomic ionization

cross-section formulas used to determine the primary flux of electrons inside the solid. All formulas in this chapter are given in atomic units ($e=m_e=h/2\pi=1$).

A. Transport theory

An energetic electron with initial energy E_0 created at depth x below a surface within a solid angle Ω_0 will undergo multiple collisions during transport in the solid. Elastic collisions as well as inelastic processes will result in angular deflections and thus determine its path to the surface. The electron may then escape from the surface into a solid angle Ω with a final kinetic energy E. In general this energy is lower than E_0 since the electron may suffer an inelastic energy loss which might be comparable to E_0 during the penetration of the material. If the initial flux of electrons per unit energy, solid angle, and path length interval is denoted F, the doubly differential electron emission probabilities for ion-induced electrons outside the solid is given by[13]

$$I_1(E,\Omega,x)=\int dE_0\int d\Omega_0\int dx' F(E_0,\Omega_0,x')\cdot P_T(E_0,\Omega_0,x-x',E,\Omega)\ . \tag{2}$$

The propagator function P_T is the probability that an electron generated at the depth x' with initial energy E_0 and direction Ω_0 will pass a layer at a depth x with final energy E and direction Ω. In general P_T could also account for cascade electron production inside the solid, but we consider the influence of cascade processes by partitioning the doubly differential electron emission probabilities $d^2P/d\Omega dE$ as follows:

$$\frac{d^2P}{d\Omega dE}(E,\Omega)=I_1(x=0)+I_2(x=0)+I_3(x=0)+\cdots\ . \tag{3}$$

In this notation I_1 describes the emission of first-generation electrons (produced by the incident ion), I_2 corresponds to the contribution from second generation electrons produced via electron-electron collisions, and so on. The cascade contributions I_n ($n>1$) may be calculated via

$$I_n(E,\Omega,x)=\int dE_0\int d\Omega_0\int dx'\int dE'\int d\Omega' I_{n-1}(E',\Omega',x')\cdot F_e(E',\Omega',x',E_0,\Omega_0)\cdot P_T(E_0,\Omega_0,x-x',E,\Omega) \tag{4}$$

with F_e as the flux of secondary electrons being created by another electron of energy E' and direction Ω'. It should be noted that under several assumptions (such as, e.g., straight-line paths, an infinite homogeneous medium, and isotropic primary electron flux) we may obtain an expression from Eqs. (2) and (3) which was derived by Spencer and Attix[25] using a model developed by Spencer and Fano.[26] Up to this point Eqs. (2), (3), and (4) are exact within the framework of a classical transport theory, but it may be seen that a few approximations are needed in order to solve Eqs. (2)–(4).

The partition in terms of cascade contributions in Eq. (3) is expected to converge rapidly since the function P_T is usually defined so that the fastest excited electron after an inelastic collision is treated as the primary particle. Therefore a secondary electron may gain at most half the incident energy, but on the average much less. This leads to a rapid decrease in the mean electron energy of I_n with increasing n until ionization is energetically forbidden or low energetic electrons from only a few surface layers may escape the solid.

The key point to the solution of Eqs. (2)–(4) is now the determination of the propagator function P_T. In principle this function may be obtained from classical trajectory Monte Carlo calculations, or Eqs. (2)–(4) may be treated completely by a Monte Carlo method,[10] as it is applied to the calculation of ion implantation distributions.[27] However, this is a time-consuming procedure, especially since the primary spectrum F is a complicated function (or implies a similarly time-consuming calculation of atomic ionization cross sections), and spectra for a broad range of final electron energies should be computed. We therefore introduce some (not too crude) approximations for the propagator function in order to perform part of the integrations in Eq. (2) analytically.

If we restrict our treatment to primary electrons with initial energies >200 eV which may escape the surface from deep inside the solid (>5 layers) and which therefore suffer multiple inelastic collisions, then the slowing down will be be determined simply by the stopping power $S(E)$, i.e., energy straggling may be neglected. [The stopping power $S(E)$ is the sum over all inelastic cross sections multiplied by the corresponding energy transfers and the atomic density.] Consider furthermore final electron energies which are high enough so that the path length influenced by angular deflections is more appropriately described by a δ function (no path length straggling for a given production and emission angles Ω_0 and Ω) than by a diffusionlike distribution (for a discussion of electron diffusion see, e.g., Ref. 13). Hence, we may separate the energy loss and angular scattering (SELAS) contribution in the propagator function. SELAS is also justified by the fact that angular scattering is caused mainly by the target nuclei, whereas the energy loss is strongly influenced by energy transfer to nonlocalized conduction-band electrons.

Under the above assumptions the propagator becomes

$$P_T(E_0,\Omega_0,l,E,\Omega)\approx\delta(E_0-E-\Delta E(l,E))\times Q\left[\frac{E+E_0}{2},l,\alpha\right], \tag{5}$$

where Q represents the probability for the scattering of an electron from an initial direction Ω_0 to the direction Ω at the surface with α being the angle between Ω_0 and Ω. The Dirac δ function is dependent on ΔE, the energy loss of an electron with final energy E after having traveled the path length l. Therefore

$$\Delta E(l,E)=\int_0^l dR\, S(E'(E,R)) . \tag{6}$$

From Eqs. (2), (5), and (6) it follows for homogeneous media of thickness $x_{\max}$ that

$$I_1(E,\Omega,x)\approx \int_{E_{\min}}^{E_{\max}} dE_0 \int d\Omega_0 \left[\frac{dl}{dx}S(E)\right]^{-1} F(E_0,\Omega_0) \times Q\left[\frac{E+E_0}{2}, l(R(E_0,E))\alpha\right] + DF(E,\Omega) \tag{7}$$

with

$$E_{\max}=E+\Delta E(l(x_{\max}-x),E) ,$$
$$E_{\min}=E+\Delta E(l(D),E) , \tag{7a}$$

and

$$R(E_0,E)=\int_{E_0}^{E} dE' S^{-1}(E') . \tag{7b}$$

It should be noted that a surface layer of thickness D was taken into account separately in Eq. (7) since no energy loss or angular scattering occurs for this layer. If we now restrict the treatment to forward angle scattering ($\alpha<90°$) the path length may be approximated by the straight-line value given by

$$l=\left|\frac{x}{\cos\theta}\right| \tag{8}$$

with θ the angle between Ω and the outward surface normal. This should be a reasonable approximation especially for those electrons which are both created and observed in the forward direction. This holds true for the majority of the forward ejected electrons. Thus it follows that

$$I_1(E,\Omega,x)\approx \left|\frac{\cos\theta}{S(E)}\right| L + DF(E,\Omega) \tag{9}$$

with

$$L=\int_{E_{\min}}^{E_{\max}} dE_0 \int d\Omega_0 F(E_0,\Omega_0) \times Q\left[\frac{E+E_0}{2}, l(R(E_0,E)),\alpha\right] \tag{9a}$$

$$=\int_{E_{\min}}^{E_{\max}} dE_0 \int_0^{\pi} d\theta_0 \sin\theta_0 F(E_0,\theta_0) M(E_0,\theta_0,E,\theta) \tag{9b}$$

and

$$M(E_0,\theta_0,E,\theta) = \int_0^{2\pi} d\phi_0 Q\left[\frac{E+E_0}{2}, l(R(E_0,E)), \alpha(\phi_0,\theta_0,\theta)\right] , \tag{9c}$$

where α is the angle between Ω and Ω_0. In Eqs. (9b) and (9c) we have used the isotropy of the primary electron flux with respect to rotations about the beam axis. This is possible when the target is not a perfect crystal, where ion channeling or electron channeling may break the symmetry (for a review of channeling effects see, e.g., Ref. 28). Equation (9c) may be solved analytically for Q defined as

$$Q(E,l,\alpha)=\begin{cases} a\sin^{-4}(\alpha_0/2) & \text{for } \alpha<\alpha_0 \\ a\sin^{-4}(\alpha/2) & \text{for } \alpha\geq\alpha_0 \end{cases} \tag{9d}$$

with

$$\alpha_0=2\arcsin\sqrt{8\pi a/(4\pi a+1)} .$$

The angular distribution function [Eq. (9d)] yields a unitary transformation and is identical to the Rutherford scattering formula for large angles and thin targets. The constant a is obtained from the Molière theory of multiple scattering[29] for a scattering angle of 180°. For small angles ($\alpha\ll\alpha_0$) multiple scattering has to be considered and for intermediate angles ($\alpha\approx\alpha_0$) the theory for plural scattering would be appropriate. However, Eq. (9d) accounts only qualitatively for the corresponding angular distributions.

In order to treat the contributions from mainly low-energy cascade electrons as defined in Eqs. (3) and (4) in a manner similar to the ion-induced electrons in Eqs. (9) the depth dependence of I_{n-1} in Eq. (4) must be neglected. This is probably a reasonable assumption for foil thicknesses of more than about ten layers. Since the angular distribution function Q in Eq. (9a) introduces a considerable broadening of the angular distributions of cascade contributions I_n for $n>1$ we replace Q by 1, so that

$$I_n(E,\Omega,x=0)\approx\frac{\rho}{2}\left[\cos\theta S^{-1}(E) \times\int_{E_{\min}}^{E_{\max}} dE_0 \int_{2E_0+I_B}^{\infty} dE' Y(E_0,E') + D\int_{2E+I_B}^{\infty} dE' Y(E,E')\right] , \tag{10}$$

where

$$Y(E_0,E')=\frac{d\sigma_e}{dE}(E_0,E')\int_0^{\pi} d\theta' \tan(\theta) I_{n-1}(E',\Omega',x=0)$$

and $d\sigma_e/dE$ is the singly differential electron-atom collision cross section. The target density ρ is given in atoms per volume element.

In this work we used the analytical solution of Eq. (9c) to calculate the energy and angular distribution of first-generation electrons at the foil surface. Since the targets used in this work have no ideally flat surface, the surface potential was taken into account simply by subtracting the corresponding energy from the kinetic energy of ejected electrons. With the stopping power formula and atomic ionization cross sections discussed in the next section, it was then possible to calculate absolute electron emission yields for the ion-solid interactions.

B. Atomic ionization cross sections

The solution of Eq. (9) requires a calculation of the primary electron flux $F(E_0,\theta_0)$. In a first approximation, F may be taken as the product of the atomic ionization cross section and the target density. These ionization cross sections are available for some cases either as experimental or theoretical data. Since the effects due to plasmon screening[30,31] or excited projectile electrons in a metal or semiconductor are not incorporated into the experimental cross-section values, we determined analytical approximations for the atomic ionization cross sections which include screening corrections. It should be noted that to date there is no atomic collision theory which yields sufficiently accurate doubly differential cross sections for high projectile charges and for projectile velocities near to the mean electron orbital velocity.[32–34] Another reason for the need of analytical cross-section formulas is the large amount of computing time (up to CPU hours) which is necessary to obtain theoretical angular distributions of ejected electrons if high electron energies are considered[35] and/or if the treatment goes beyond first-order perturbation theory .[36,37] In the following we give analytical expressions for total and singly differential electron emission cross sections which may be obtained from fundamental ion-atom collision theories. Semiempirical corrections for effects which are incorporated only in higher-order theories are also included. The doubly differential cross sections are given by semiempirical formulas and are based on the singly differential cross sections, which are accurate to within about 40%.

The plane-wave Born approximation (PWBA) yields doubly differential cross sections which are in very good agreement with experimental data[35] for high projectile velocities and low charges. The Born approximation as given by Bates and Griffing[38] depends, for a certain transition and energies above the ionization threshold, only on the binding energy I_B and the reduced projectile energy

$$T_P=\frac{E_P}{M_P}\ , \tag{11}$$

where E_P and M_P are the kinetic energy and mass of the projectile (in atomic units). A fit to the PWBA cross sections for K-shell ionization by bare projectiles gives

$$\sigma_{\rm tot}=500n_B\left[\frac{Z_P}{I_B}\right]^2 \times\frac{x^4}{1+c_1x+c_2x^2+c_3x^3c_4+c_5x^5/\ln(47.1x)}\ , \tag{12}$$

where $x=2T_p/I_B$, $c_1=13.8$, $c_2=18$, $c_3=208$, $c_4=22$, and $c_5=256$.

The projectile nuclear charge is denoted Z_P and n_B is the number of electrons in the shell with binding energy I_B. The above expression fits the PWBA values to within about 15% for $x>0.1$ with the correct asymptotic behavior. The total cross sections calculated with Eq. (12) agree to within 30% with experimental ionization cross sections for highly energetic ions ($Z_P=1$ to 10) and He K-, Ar M-, Ar L-, and Ar K-shell electrons.[34,35]

It should be noted that the PWBA treatment is incorrect for x less than about $2Z_T$ since polarization effects, electron capture, and molecular effects come into play.[32,33,35,37] If quasimolecular processes such as promotion are important, perturbational treatments (such as the PWBA) may yield cross sections with order of magnitude errors.[39] However, the region of validity of the PWBA may be extended (for a few cases down to very low incident energies) by applying a binding correction to I_B,[40,41] which is then a function of the mean impact parameter and the projectile velocity. Such a correction was applied, but resulted in only small effects ($<20\%$) for the highly energetic projectiles investigated in this work. Thus the corresponding formulas will not be discussed here.

The singly differential cross section $d\sigma/dE$ may be subdivided into three partial cross sections corresponding to different electron-production mechanisms according to

$$\frac{d\sigma}{dE}=\frac{d\sigma_H}{dE}+\frac{d\sigma_S}{dE}+\frac{d\sigma_C}{dE}\ . \tag{13}$$

The PWBA includes a contribution from hard collisions $d\sigma_H/dE$ (dominant for about $T_P<100I_B$) corresponding to large momentum transfer to the emitted electrons at small impact parameters compared to the mean orbital radius of the initial state. The PWBA also includes a contribution from soft collisions $d\sigma_S/dE$ at large impact parameters. It should be noted that this term does not occur in purely classical collision theories. The expression $d\sigma_C/dE$ stands for capture to the projectile continuum. This particular mechanism is not included in the PWBA for direct ionization, and may be calculated within the framework of capture theories.[42,43] However, it has been found that a more accurate description of the corresponding forward electron emission is only possible when the influences of the target and projectile nuclear potentials are treated coherently.[33] Since this is possible only for a few theoretical models[36,37] and since no analytical *ab initio* expressions have been derived for $d\sigma_C/dE$, we performed a fit to the difference between experimental and PWBA values for $d\sigma_C/dE$.

In the classical binary-encounter approximation (BEA) for high incident energies, $d\sigma_H/dE$ may be written as[44–46]

$$\frac{d\sigma_H}{dE}(E)=2\pi\frac{n_BZ_P^2}{v_P^2}(\Delta E^{-2}+\tfrac{4}{3}I_B\Delta E^{-3}) \tag{14}$$

with $\Delta E=I_B+E$ if the velocity distribution of the initial state is represented by the mean orbital velocity and $\Delta E<E_B$, where $E_B=4T_P$ is the maximum energy transfer between a heavy projectile and an electron at rest. It should be noted that Eq. (14) approaches the Rutherford formula for initially free electrons ($I_B\to0$).

The doubly differential cross sections $d^2\sigma_H/d\Omega dE$ for hard (binary) collisions may be approximated as follows:

$$\frac{d^2\sigma_H}{d\Omega dE}(\theta,E)=d_0\left\{1.33\exp(-|\theta-\theta_B|/\Delta\theta_B-0.288)+d_1\left[1-\sin\left[\frac{\pi}{2}(\theta-\theta_B)/(\pi-\theta_B)\right]\right]\right.$$
$$\left.+0.5(1+I_B/T_P(E/I_B)^{2.8})(I_B/I\Delta E)^2\right\} \quad (15)$$

with

$$\Delta\theta_B(E)=1.6\arcsin[I_B/(I_B+0.5E)] \quad (15a)$$

and

$$\theta_B(E)=\arccos[\sqrt{\Delta E/E_B+0.22T_P^{0.7}/(T_P+E)}] \quad . \quad (15b)$$

The first term in Eq. (15) describes the binary-encounter peak with an angular width $\Delta\theta_B$ centered at the angle θ_B with respect to the incident beam. The parameter d_0 serves to normalize the cross sections $d^2\sigma_H/d\Omega dE$ to $d\sigma_H/dE$. The second term in Eq. (15) approximates a kinematic forward electron ejection as determined by the initial electron velocity distribution. The parameter d_1 approaches zero for high ejection energies or for vanishing binding energies I_B. The third term is dominant at backward ejection angles and stems from the Coulomb deflection of emitted electrons in the field of the target nucleus.[45] It should be noted that Eq. (15) converges to the Rutherford scattering formula for vanishing binding energies and high electron energies [see Eq. 15(b)].

The cross section $d^2\sigma_S/d\Omega dE$ (corresponding to soft collisions) becomes important for high incident energies and low electron ejection energies. This part of the ionization cross section may be parametrized (for K-shell ionization) as[47–49]

$$\frac{d^2\sigma_S}{d\Omega dE}(\theta,E)=d_2Z_P^2\Delta E^{-(2.9+I_B^{0.08})}$$
$$\times[2-\beta(3\cos^2\theta-1)] \quad . \quad (16)$$

For initial states with high orbital angular momentum quantum numbers (e.g., p or d states) the dependence of ΔE is somewhat stronger than that given in Eq. (16). The constant β was set to 0.5 for the present calculation, and the function d_2 approaches zero for $T \ll I_B$.

The projectile may carry bound electrons during the passage through the solid in which case its Coulomb potential would be partially screened. We applied screening corrections to the singly differential cross sections by assuming that the projectile electrons may be represented by an exponential density distribution (characterized by an effective projectile charge).[19,38] Since the screening corrections are small (of the order of 10–30% for the cases considered here) we will not discuss the corresponding formulas. The influence on the ion-induced electron spectra due to plasmon scattering of the projectile charge by conduction-band electrons was estimated to be less than 5% at these high incident energies. Although both contributions are not very significant, they were both included in our calculations in an approximate way.

Figures 3 and 4 display the electron angular distribution for six electron energies in 100 MeV Ne^{10+} incident on He and Ar targets. It is seen that the cross sections calculated with our semiempirical formulas yield a relatively good agreement with the experimental results, even though the absolute cross-section values vary over several orders of magnitude. The especially good agreement between experimental and semiempirical data for the multielectron target Ar for energies above 10 eV indicates that the semiempirical ionization cross sections for highly ionized Ne ions incident on a C target should be uncertain by less than a factor of 2 for doubly differential cross sections, and less than 20% for total cross sections.

In order to solve Eqs. (6), (7), and (9) an electron stopping power has to be defined. For high electron energies

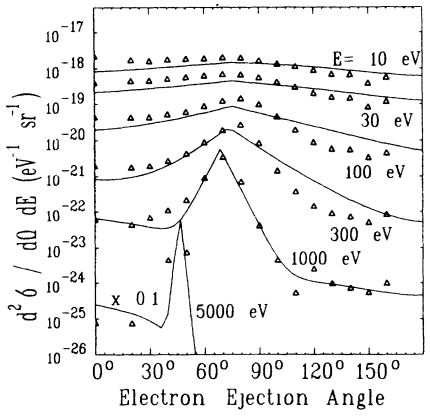

FIG. 3. Experimental doubly differential electron spectra (Ref. 34) for 100-MeV Ne^{10+} + He, compared to the semiempirical cross sections used in this work (solid lines).

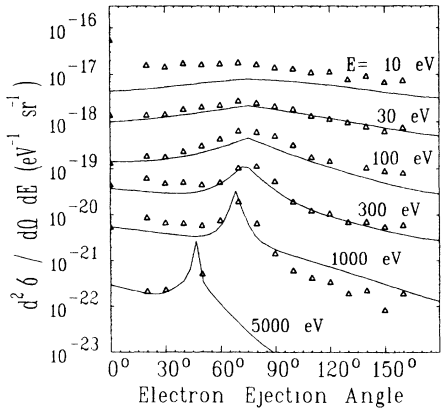

FIG. 4. Experimental doubly differential electron spectra (Ref. 34) for 100-MeV Ne^{10+} + Ar, compared to the semiempirical cross sections used in this work (solid lines).

($E \gg Z_T^2$) the Bethe-Bloch formula[50] should be a good approximation. However, for lower electron energies, this formula is expected to fail since the ionization thresholds of the different target shells and plasmon excitations come into play. Therefore we used the more exact approximation to the stopping power dE/ds for electrons

$$\frac{dE}{ds} = \frac{dE_p}{ds} + \sum_j \sigma_j E_j \tag{17}$$

with dE_P/ds being the plasmon stopping power as defined by Pines and Bohm.[30] The electron impact ionization cross section for a target shell j, σ_j, was obtained from a semiempirical formula by Casnati *et al.*[51] and is known to be a good approximation for ionization above the threshold.[52] The mean excitation energy E_j was estimated by assuming a $\Delta E^{-2.5}$ dependence [see Eq. (14)] for the singly differential cross section which is expected to be a good approximation. It should be noted that the deviation of Eq. (17) from the Bethe-Bloch formula is less than 10% for a C target at high electron energies, and exceeds 50% for electron energies below 150 eV.

IV. RESULTS AND DISCUSSION

In order to give an overview of the characteristics of electron emission from solid targets induced by fast heavy-ion beams, we present in Table I some specific quantities obtained from the experimental data. It should be noted that the mean electron energy for forward ejection angles exceeds 1 keV for incident energies above 3.5 MeV/u. About 30 electrons are emitted per incident ion. Thus the energy deposition in the flux of emitted electrons exceeds 30% of the total stopping power estimated with the Bethe-Bloch formula for 20 $\mu g/c^2$ C foils. Model calculations in the SELAS approximation show that all shells contribute nearly equally to the electron spectra at high electron energies. Only at energies below 200 eV do the outer shells (the conduction band) dominate the spectra, and at energies below about 50 eV there is a strong influence from the surface layers and electron cascades [see Eqs. (3) and (10)].

In Table I we also give absolute Auger electron emission yields. These quantities are subject to uncertainties of about 50%. This was estimated with different functional dependencies of the subtracted continuous background due to secondary electrons. The C-*KLL* Auger electrons constitute 3–6 % of the total number of emitted electrons. Since C-*KLL* Auger electrons may escape the solid only from about eight layers below the surface, the absolute values in Table I may depend on surface properties, such as roughness. It may also be seen from Table I that the Auger electron yields for forward ejection are larger than the values for backward angles. This was attributed in an earlier publication[53] to secondary electrons leading to K-shell ionization near the exit (forward) surface to the foil.

Figure 5 displays the same experimental electron spectra as in Fig. 1. The experimental data are fitted to the theoretical predictions at angles $>0°$ and electron energies between 2 and 2.5 keV. It should be noted that all other experimental data presented in this paper are absolute values determined according to Sec. II. The dotted lines in Fig. 5 are calculated in the SELAS approximation for target electrons as described in Sec. III. The solid lines include additional contributions from different projectile shells. The population of the projectile K shell (P_K) and the population of all other levels ($P_n = P_0 n^{-3}$) were treated as independent fit parameters. The corresponding electron-loss cross sections were calculated as described in Sec. III B and were corrected for electron-electron interaction contributions—the so-called antiscreening. The resulting cross sections were transformed from the projectile frame into the laboratory frame and treated in the SELAS approximation (see Sec. III A). The results of the fits for P_K and P_0 are discussed in detail elsewhere.[54]

The contribution of ionized projectile electrons has its maximum at forward angles and results in a cusp-shaped peak at zero degrees for an electron velocity equal to the projectile velocity. The experimentally observed C-*KLL* Auger peaks at energies below 260 eV are not taken into account in our calculations. In light of the approximations involved in the present SELAS model there is remarkably good agreement between experimental and theoretical electron emission yields. It should be kept in mind that the calculations are expected to be most accurate for forward ejection angles and energies above a few hundred eV. However, the largest discrepancy is found for forward ejection angles and energies somewhat below the cusp peak.

Figures 6 and 7 display absolute experimental electron

TABLE I. Absolute emission yields and mean electron energies for Ne q_i^+ ions incident on carbon foils of thickness t as a function of projectile energy E_p. The final charge state is denoted q_f. The mean electron energy E and the emission yield P correspond to all ejected electrons, and the emission yield A to Auger electrons only. The subscripts F and B correspond to the fractions being emitted in forward and backward directions, respectively.

E_p (MeV)	t ($\mu g/cm^2$)	q_i	q_f[a]	E_F (eV)	E_B (eV)	P_F	P_B	A_F	A_B
70	20	10	8.92	940	280	32[b]	10[b]	0.76[b]	0.42[b]
100	20	10	9.16	1150	470	26	7.6	1.22	0.81
170	100	7	9.44	1600	620	16	6.2	0.61	0.32

[a]Calculated using Eq. (1).

[b]Relative values normalized to $P_B = 10$.

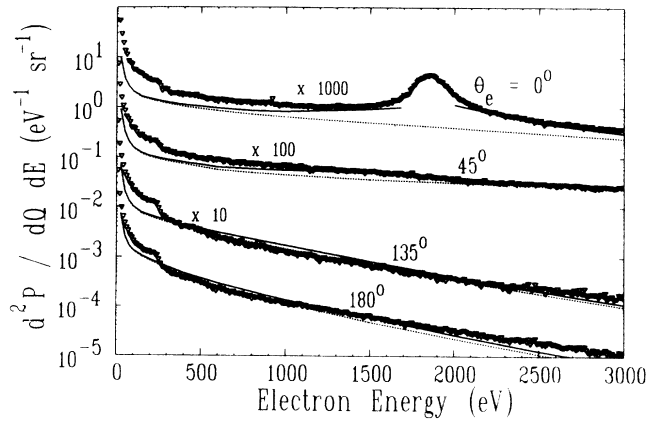

FIG. 5. Measured electron-energy spectra for different ejection angles in 70-MeV $Ne^{10+}+20\ \mu g/cm^2$ C-foil collisions normalized to the predictions of the present SELAS model. Dotted lines: results of the present SELAS calculations for target electrons; solid lines: SELAS theory including emission of projectile electrons.

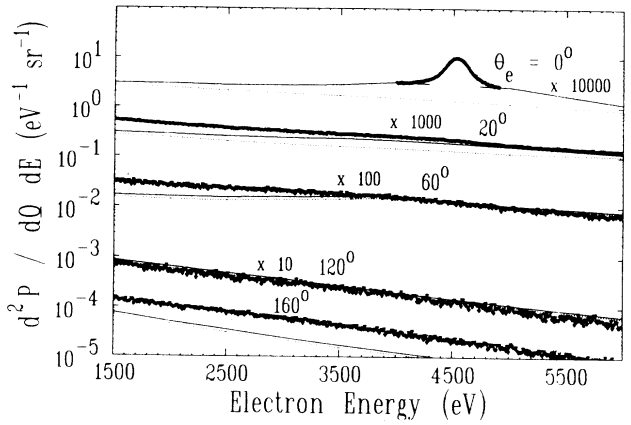

FIG. 7. As in Fig. 6 for 170-MeV $Ne^{7+}+100\ \mu g/cm^2$ C-foil collisions.

emission yields in comparison with results of the SELAS model. The general tendencies are similar to those described above (see Fig. 5), but the theoretical results were found to underestimate the electron emission yields by a factor of 2–3 for large backward angles ($>120°$). This might be a result of the macroscopic target structure. The target foils used in this work have a relatively well-defined thickness, but electrons emitted at 90° see a nearly infinite target thickness and thus may be scattered into backward angles with a much higher probability (50%) than predicted by Eq. (9d). This effect might be strongly reduced for 70-MeV $Ne^{10+}+C$ since the mean electron energy and therefore the escape depth is smaller than in the other cases.

A common feature of Figs. 5–7 is the deviation between experimental and theoretical results for forward ejection angles and energies below the cusp peak. This deviation reaches a factor of 5 for 100-MeV $Ne^{10+}+C$ foil. Since the theory yields too low results in all cases we might speculate that an electron production mechanism was neglected in the present treatment. We can exclude collective electron production mechanisms since the coupling between, e.g., plasmons and single electrons is relatively weak, and a *simultaneous* decay of about 100 plasmons would be necessary to explain the observed energies of up to a few keV. Another mechanism not fully taken into account is the capture of target electrons into the projectile-centered continuum (ECC). However, the corresponding electron spectra should be similar to electron-loss spectra from projectile Rydberg states.

A strong influence of the ECC was excluded by our fit of projectile-state population numbers, since even if we used the population number of each state ($n=1,\ldots,6$) as a free parameter, the agreement between experiment and theory for electron energies below the cusp peak would not be improved.

The most probable explanation for an enhancement of forward ejected electrons below the cusp is attributed to a collective transport mechanism. The highly charged projectile leads to ionization, and thus to a reduction of the electron density along its path through the solid. It should be emphasized that more than one electron per layer will be ionized by the projectile. Electrons with velocities near to the projectile velocity will be focused towards zero degrees by the resulting positively charged track behind the projectile. The decreased electron density on this track would also result in a reduction of the stopping power. Thus, once an electron follows the projectile, it will be focused to zero degrees and may reach the surface from deep inside the solid because of the reduced stopping power along the projectile path.

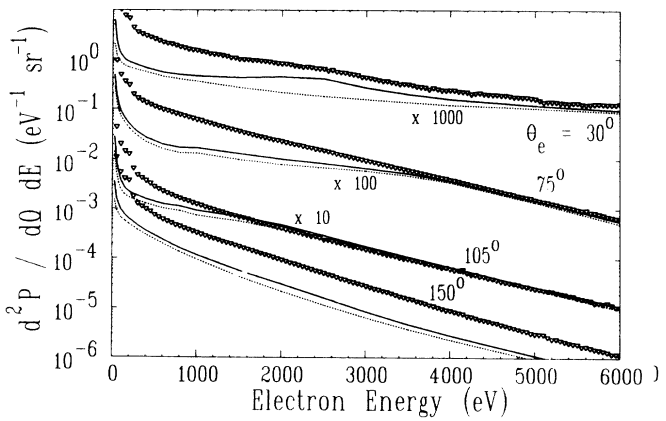

FIG. 6. Measured absolute electron-energy spectra for different ejection angles in 100-MeV $Ne^{10+}+20\ \mu g/cm^2$ C-foil collisions. Dotted lines: results of the present SELAS calculations for target electrons; solid lines: SELAS theory including emission of projectile electrons.

V. CONCLUSION

Electron spectra resulting from fast heavy-ion bombardment of thin C foils have been investigated experimentally and theoretically. Absolute electron emission

yields have been determined with an uncertainty of about ±25% for electron energies from 10 eV to 6 keV and ejection angles ranging from 0° to 180°. A theoretical model was developed based on the SELAS approximation (separation of energy loss and angular scattering). There are discrepancies between experiment and theory for large backward angles (> 120°) which are assigned to specific approximations in the transport theory. However, at intermediate ejection angles and especially at high electron energies there is very good agreement between experiment and theory. At forward ejection angles and electron velocities somewhat below the projectile velocity there is a discrepancy between theory and experiment which might be an indication of a breakdown in the independent electron model, and thus of the importance of collective effects in the case of heavy-ion–solid interactions.

Further work is needed theoretically and experimentally to identify collective effects in ion-solid interactions. A theoretical improvement which seems to be important is a proper treatment of the transport of electrons from inside the solid to the surface in the presence of the positively charged track behind the incident ion. Experimentally there is a need for data to be taken for different collision systems in the investigated regime of incident velocities. It might also be possible to improve the accuracy of the measurements so that theoretical methods may be tested in the finest details.

ACKNOWLEDGMENTS

We would like to thank J. Burgdörfer, J. Briggs, and U. Thumm for helpful and stimulating discussions. We would also like to thank U. Stettner for his help in the preparation of the experiments.

*On leave from University of Lund, Lund, Sweden.

[1]D. Schneider, H.-C. Werner, D. Ridder, M. Prost, R. DuBois, and N. Stolterfoht, in *Proceedings of the Surface Analysis 79 Conference,* edited by D. Štulik (Czechóslovak Scientific and Technical Society Branch of the Central Research Institute, Skoda Plzeň, Czechoslovakia, 1979), pp. 7/1–7/10.

[2]K. O. Groeneveld, R. Mann, W. Meckbach, and R. Spohr, Vacuum **25**, 9 (1974).

[3]F. Folkmann, K. O. Groeneveld, R. Mann, G. Nolte, S. Schumann, and R. Spohr, Z. Phys. A **275**, 229 (1975).

[4]R. Bruch, D. Schneider, W. H. E. Schwarz, M. Meinhart, B. M. Johnson, and K. Taulbjerg, Phys. Rev. A **19**, 587 (1979).

[5]J. Schader, B. Kolb, K. D. Sevier, and K. O. Groeneveld, Nucl. Instrum. Methods **151**, 563 (1978).

[6]P. B. Needham, Jr., T. J. Driscoll, C. J. Powell, and R. J. Stein, Appl. Phys. Lett. **30**, 357 (1977).

[7]C. J. Powell, R. J. Stein, P. B. Needham, Jr., and T. J. Driscoll, Phys. Rev. B **16**, 1370 (1977).

[8]R. A. Baragiola, P. Ziem, and N. Stolterfoht, J. Phys. B **9**, L447 (1976); and, in *Proceedings of the Second International Conference on Inner-Shell-Ionization Phenomena,* edited by W. Mehlhorn and R. Brenn (Universität Freiburg, Freiburg, 1976), pp. 109–111.

[9]R. E. Pferdekämpfer and H.-G. Clerc, Z. Phys. A **275**, 223 (1975).

[10]L. H. Toburen, W. E. Wilson, and H. G. Paretzke, Phys. Rev. A **25**, 713 (1982).

[11]D. Schneider, R. Kudo, and E. Kanter, Nucl. Instrum. Methods B **10**, 113 (1985).

[12]L. Fiermanns, J. Vennik, and W. Dekeyser, *Electron and Ion Spectroscopy of Solids* (Plenum, New York, 1978).

[13]S. Tougaard and P. Sigmund, Phys. Rev. B **25**, 4452 (1982).

[14]K. Siegbahn, C. Nordling, G. Johannson, J. Hedman, P. F. Hedin, K. Hamptin, U. Gelius, T. Bergmark, L. O. Werme, R. Mann, and Y. Baer, *ESCA Applied to Free Molecules* (North-Holland, Amsterdam, 1969).

[15]W. Schäfer, H. Stöcker, B. Müller, and W. Greiner, Z. Phys. B **36**, 319 (1980).

[16]M. Burton, K. Funabashi, R. R. Hentz, P. K. Ludwig, J. L. Magee, and A. Mozumder, *Transfer and Storage of Energy by Molecules* (Wiley-Interscience, New York, 1969), Vol. I, Chap. 4.

[17]N. Stolterfoht, Z. Phys. **248**, 81 (1971).

[18]D. Schneider, W. Zeitz, R. Kowallik, G. Schiwietz, T. Schneider, N. Stolterfoht, and U. Wille, Phys. Rev. A **34**, 169 (1986).

[19]G. Schiwietz, D. Schneider, and J. Tanis, Phys. Rev. Lett. **59**, 1561 (1987).

[20]Estimated with the TRIM code (see also Ref. 27).

[21]V. S. Nikolaev and I. S. Dmitriev, Phys. Lett. **28A**, 277 (1968).

[22]H.-D. Betz, Rev. Mod. Phys. **44**, 465 (1972).

[23]S. Datz, C. D. Moak, O. H. Crawford, H. F. Krause, P. F. Dkittner, J. Gomez del Campo, J. A. Biggerstaff, P. D. Miller, P. Hvelplund, and H. Knudsen, Phys. Rev. Lett. **40**, 843 (1978).

[24]U. Wille and R. Hippler, Phys. Rep. **132**, 129 (1986).

[25]L. V. Spencer and F. H. Attix, Radiat. Res. **3**, 239 (1955).

[26]L. V. Spencer and U. Fano, Phys. Rev. **93**, 1172 (1954).

[27]J. P. Biersack, Nucl. Instrum. Methods B **19**, 32 (1987).

[28]D. S. Gemmell, Rev. Mod. Phys. **46**, 129 (1974).

[29]G. Molière, Z. Naturforsch. 3a, 79 (1948).

[30]D. Bohm and D Pines, Phys. Rev. **82**, 625 (1981); **92**, 609 (1953); D. Pines and D. Bohm, Phys. Rev. **85**, 338 (1952); D. Pines, Phys. Rev. **92**, 626 (1953).

[31]W. Brandt and J. Reinheimer, Phys. Rev. B **2**, 3104 (1979).

[32]G. Schiwietz, Phys. Rev. A **37**, 370 (1988).

[33]N. Stolterfoht, D. Schneider, J. Tanis, H. Altevogt, A. Salin, P. D. Fainstein, R. Rivarola, J. P. Grandin, J. N. Scheurer, S. Andriamonje, D. Bertault, and J. F. Chemin, Europhys. Lett. **4**, 899 (1987).

[34]G. Schiwietz, H. Platten, D. Schneider, T. Schneider, W. Zeitz, K. Musiol, R. Kowallik, and N. Stolterfoht, Hahn-Meitner-Institut Report No. B-477 (unpublished).

[35]S. T. Manson, L. H. Toburen, D. H. Madison, and N. Stolterfoht, Phys. Rev. A **12**, 60 (1975); M. E. Rudd, L. H. Toburen, and N. Stolterfoht, At. Data Nucl. Data Tables **18**, 413 (1976).

[36]P. D. Fainstein, V. H. Ponce, and R. D. Rivarola, J. Phys. B **21**, 287 (1988).

[37]G. Schiwietz and W. Fritsch, J. Phys. B **20**, 5463 (1987).

[38]D. R. Bates and G. Griffing, Proc. Phys. Soc. London, Sect. A **66**, 961 (1953).

[39]G. Schiwietz, B. Skogvall, J. Tanis, and D. Schneider, Phys. Rev. A **38**, 5552 (1988).
[40]A. Jakob, D. Trautmann, F. Rösel, and G. Baur, Nucl. Instrum. Methods **232**, 218 (1984).
[41]W. Brandt, R. Laubert, and I. Sellin, Phys. Lett. **21**, 518 (1966).
[42]A. Salin, J. Phys. B **2**, 631 (1969).
[43]J. Macek, Phys. Rev. A **1**, 235 (1970).
[44]R. C. Stabler, Phys. Rev. **133**, A1268 (1964).
[45]M. Grizinski, J. Phys. B **20**, 4741 (1987).
[46]L. Vriens, in *Case Studies in Atomic Physics*, edited by E. W. McDaniel and M. R. C. McDowell (North-Holland, Amsterdam, 1969), Vol. 1, p. 335.
[47]H. Bethe, Ann. Phys. (Leipzig) **5**, 325 (1930); M. Innokuti, Rev. Mod. Phys. **43**, 297 (1971).
[48]Y. K. Kim, Phys. Rev. A **6**, 666 (1972).
[49]M. Innokuti, Y. K. Kim, and R. L. Platzmann, Phys. Rev. **164**, 55 (1967).
[50]F. Bloch, Z. Phys. **81**, 363 (1933).
[51]E. Casnati, A. Tartari, and C. Baraldi, J. Phys. B **15**, 627 (1982).
[52]H. Platten, G. Schiwietz, and G. Nolte, Phys. Lett. **107A**, 83 (1985).
[53]G. Schiwietz, D. Schneider, J. P. Biersack, N. Stolterfoht, D. Fink, A. Mattis, B. Skogvall, H. Altevogt, V. Montemayor, and U. Stettner, Phys. Rev. Lett. **61**, 2677 (1988).
[54]G. Schiwietz, *Radiation Effects and Defects in Solids* (Gordon and Breach, London, 1990).